Limitations and Accuracy of a Continuous Reduced-Order Model for Modular Multilevel Converters

Andres M. Lopez, *Student Member, IEEE*, Daniel E. Quevedo, *Senior Member, IEEE*, Ricardo P. Aguilera, *Member, IEEE*, Tobias Geyer, *Senior Member, IEEE*, and Nikolaos Oikonomou, *Student Member, IEEE*

***Abstract*—This paper analyzes the limitations of a reduced-order model for modular multilevel converters (MMCs) by elucidating the relation between its accuracy, operating frequency, and converter parameters. A reduced-order simplifies the analysis of the MMC and thereby may provide additional information about the converter behavior. However, the accuracy of such model depends on several factors. In this paper, the effect of approximating the converter as a continuous system by neglecting quantization issues associated with having a finite number of modules is studied in detail. The analysis is done based on Fourier-series approximations with which it is possible to elucidate the relationship between the resonant frequencies of the MMC and the error of the reduced-order model. With the Fourier approximation, it is also possible to characterize resonant frequencies of the converter, both numerically and analytically, in terms of the converter parameters. The results can serve as a tool to identify situations when the reduced-order model produces good and also less accurate approximations especially when a low number of modules is available.**

***Index Terms*—DC-AC power conversion, frequency domain analysis, modeling, power converter.**

I. Introduction

RECENTLY, MMCs have become a popular power converter topology. Numerous studies have been carried out for this converter due to its advantages in high-power and high-voltage applications. In addition to this, its modularity, low-distortion and high-voltage capabilities are some other characteristics that make the MMC a very important topology for industry. Some of the industrial applications of the MMC include wind energy conversion, HVdc grids, and medium-voltage drives [1]–[3]. Due to its relevance, several studies have proposed different techniques to improve performance and address important issues. These include modulation techniques [4]–[6], voltage balancing techniques [7], optimal capacitor ripple reduction [8], [9], several control approaches [10]–[13], and energy quality and reliability [14], [15]. All of these works also aim to understand operation principles of MMCs.

MMCs are complex power converters that exhibit a highly nonlinear behavior. In order to understand their operational principles and analyze the converter, it is important to be able to obtain relatively simple mathematical expressions that not only describe the converter accurately, but also allow one to obtain insight into the behavior of the system. This insight can be used as a guideline for different design purposes such as selection of references for control, injection of current harmonics for voltage ripple reduction, or selection of control laws for different applications [16].

Several modeling approaches for the MMC have been presented in the literature. Some of these approaches are designed for simulation purposes with various levels of complexity [17]–[19]. The simpler models often neglect some of the dynamics of the converter and do not consider power losses, opening the path for more accurate methods to be proposed [20]. For a more detailed analysis of the converter a more complex model is required. In [21] and [22], models that aim to obtain detailed information about the converter losses and behavior in steady state are proposed. However, important information about the dynamics of the MMC cannot be obtained. In other works [23]–[27], more detailed continuous dynamical models of the MMC are presented. These models exhibit a reduced number of state space and control variables while maintaining the nonlinearities of the MMC. In [28] and [29], these kind of models have been used to determine open-loop control strategies that use calculated steady-state values and estimated voltage ripple values to achieve energy control with asymptotical stability. In general, all these models are represented in the abc frame, complicating the analysis of the converter due to the multiplication of two time-varying signals. In [30], a more convenient representation in the dq frame is presented. However, the analysis is carried out for a linear case using only up to a second-order harmonic.

This paper further extends the concept in [31] and analyzes the impact of additional harmonic components in the converter model as well as in the control signals in more detail. This is

Manuscript received May 19, 2017; accepted July 16, 2017. Date of publication August 21, 2017; date of current version March 5, 2018. Recommended for publication by Associate Editor M. Saeedifard. *(Corresponding author: Andres M. Lopez.)*

A. Lopez and D. E. Quevedo are with the University of Paderborn, Paderborn 33098, Germany (e-mail: andres.lopez@upb.de; dquevedo@ieee.org).

R. P. Aguilera is with the University of Technology Sydney, Sydney, NSW 2007, Australia (e-mail: raguilera@ieee.org).

T. Geyer and N. Oikonomou are with ABB's Corporate Research Center, Baden 5405, Switzerland (e-mail: tobias.geyer@ch.abb.com; nikolaos.oikonomou@ch.abb.com).

Color versions of one or more of the figures in this paper are available online at http://ieeexplore.ieee.org.

Digital Object Identifier 10.1109/TPEL.2017.2743006

particularly useful in the case where the number of modules are low and the quantization in the control signals is neglected in order to obtain a continuous-system representation. An interesting phenomenon is that the accuracy of the model in [23] (reduced-order model) is greatly affected when the operating frequency of the converter matches some specific frequencies. Following an analytical procedure, expressions for some of the frequencies where the error of the reduced-order model is more significant are presented, constituting one of the main contributions of this paper. These frequencies are poorly damped resonant modes that depend on the converter parameters and the harmonic content of the inputs. In [32] and [33], it is shown that these poorly damped modes can generate instability in a closed-loop control strategy. The method presented in this paper is a straightforward alternative to identify such frequencies and therefore it also has potential use for stability analysis [34]. This paper focuses on analyzing and clarifying the accuracy of the reduced-order model and its relationship with the converter parameters.

Several approaches are used in this paper in order to estimate the frequency response of the MMC; these include numerical solutions and also derivation of analytical expressions based on Fourier expansion and linearized models. The subsequent analysis shows that the accuracy of the reduced-order model is low close to the resonant frequencies of the converter due to the additional frequency components introduced by quantization effects. This produces a modulation effect that displaces the resonant frequencies of the reduced-order model (when continuous signals are used) in comparison with those of the full-order MMC (with quantization). This generates differences in where the amplitude peak related to the resonance is located, producing inaccuracies. With sufficient knowledge about the resonant frequencies, it is possible to determine beforehand if the response of the reduced-order model is accurate enough. This information can be helpful when designing an MMC based on the reduced-order model. The verification of this analysis in this paper is limited to a simulation environment.

This paper is organized as follows. Sections II and III present the MMC and the reduced-order model, respectively. Section IV discusses issues related to the application of the reduced-order model such as use of continuous control signals, voltage imbalances, and blocking modes. Sections V and VI estimate the frequency response of the MMC using an approach based on linearization and a Fourier-series expansion, respectively. Finally, Section VII draws conclusions.

II. Modular Multilevel Converter

The MMC is a power-converter topology, which transforms the waveform of an electrical variable from dc to ac or vice versa (see Fig. 1) [1], [35].

In order to control the MMC, the switch positions of each module shown in Fig. 1 can be chosen independently to be one of two possible values: "Inserted" or "not-inserted." A module is considered "inserted" when its voltage (V_i^M) is equal to the voltage of its respective capacitor. Conversely, a module is considered "not-inserted" when its voltage (V_i^M) is equal to 0.

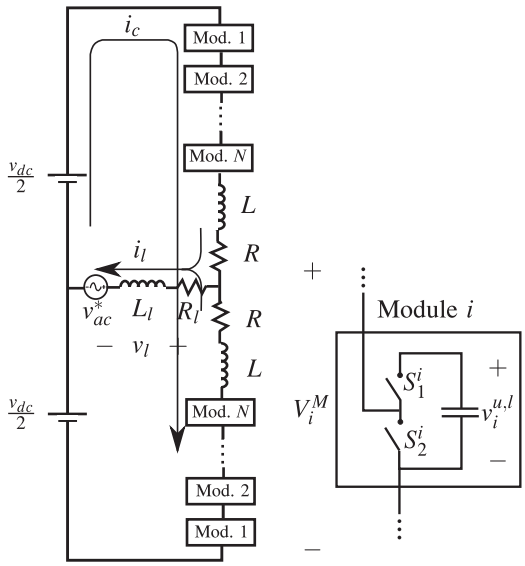

Fig. 1. MMC with N modules per arm. Here, v_l denotes the output voltage of the converter, i_l stands for the load current, and i_c for the circulating current. S_1^i and S_2^i are the positions of the switches and $v_i^{u,l}$ and V_i^M describe the voltage of the capacitors and the modules, respectively.

The desired waveforms of output currents and voltages of the MMC are sinusoidal and can be defined as follows:

$$i_l(t) = \hat{i}_l \cos(\omega t + \phi) \tag{1}$$

$$v_l(t) = \hat{v}_l \cos(\omega t) \tag{2}$$

where $\hat{i}_l$ is the amplitude of the output current and ω represents the angular frequency. The phase angle ϕ and the voltage amplitude $\hat{v}_l$ can be calculated depending on v^*_{ac}, R_l, and L_l.

Using electrical circuit analysis methods, an MMC (see Fig. 1) with N submodules per arm can be described by the following state-space model:

$$\dot{x}(t) = \mathcal{A}\left(\vec{\mu}^u(t), \vec{\mu}^l(t)\right) x(t) + \mathcal{B}[v_{\text{dc}} \quad v^*_{\text{ac}}]^T \tag{3}$$

where

$$x(t) \triangleq \left[\, i_c(t)\ i_l(t)\ v_1^u(t) \cdots v_N^u(t)\ v_1^l(t) \cdots v_N^l(t) \,\right]^T \tag{4}$$

is the system state. In (4), i_c is the circulating current, whereas v_i^u and v_i^l represent the capacitor voltages of the ith module of the upper (u) and lower (l) arms.

In (3), $\vec{\mu}^u(t)$ and $\vec{\mu}^l(t)$ represent the control signals for the modules in the upper and lower arms. Each individual component of these control signals can take the value of 1 (module inserted) or 0 (module not inserted)

$$\vec{\mu}^u(t) \triangleq \left[\, \mu_1^u(t) \quad \cdots \quad \mu_N^u(t) \,\right]^T,\ \mu_i^u(t) \in \{0,1\} \tag{5}$$

$$\vec{\mu}^l(t) \triangleq \mu_1^l(t) \quad \cdots \quad \mu_N^l(t)^T,\ \mu_i^l(t) \in \{0,1\}. \tag{6}$$

The matrix $\mathcal{A}\left(\vec{\mu}^u(t), \vec{\mu}^l(t)\right)$ is defined as follows:

$$\mathcal{A}\left(\vec{\mu}^u(t), \vec{\mu}^l(t)\right) \triangleq \begin{bmatrix} \mathcal{A}_{1,1} & \mathcal{A}_{1,2}\left(\vec{\mu}^u(t), \vec{\mu}^l(t)\right) \\ \mathcal{A}_{2,1}\left(\vec{\mu}^u(t), \vec{\mu}^l(t)\right) & 0 \end{bmatrix} \tag{7}$$

with

$$\mathcal{A}_{1,1} = \begin{bmatrix} -\frac{R}{L} & 0 \\ 0 & -\frac{R+2R_l}{L+2L_l} \end{bmatrix}$$

$$\mathcal{A}_{1,2}\left(\vec{\mu}^u(t), \vec{\mu}^l(t)\right) = \begin{bmatrix} -\frac{1}{2L}\vec{\mu}^u(t)^T & -\frac{1}{2L}\vec{\mu}^l(t)^T \\ -\frac{1}{L+2L_l}\vec{\mu}^u(t)^T & \frac{1}{L+2L_l}\vec{\mu}^l(t)^T \end{bmatrix}$$

$$\mathcal{A}_{2,1}\left(\vec{\mu}^u(t), \vec{\mu}^l(t)\right) = \begin{bmatrix} \frac{1}{C}\vec{\mu}^u(t) & \frac{1}{2C}\vec{\mu}^u(t) \\ \frac{1}{C}\vec{\mu}^l(t) & -\frac{1}{2C}\vec{\mu}^l(t) \end{bmatrix}. \quad (8)$$

Finally, $\mathcal{B}$ is given by

$$\mathcal{B} \triangleq \begin{bmatrix} \frac{1}{2L} & 0 & \cdots & 0 \\ 0 & -\frac{2}{L+2L_l} & \cdots & 0 \end{bmatrix}^T. \quad (9)$$

III. Reduced-Order Model

The MMC is a discontinuous system with multiple switchable inputs, as shown in (3). These discontinuities complicate the analysis of the converter. In order to simplify the analysis and obtain expressions for the variables of interest, this section investigates a model introduced and validated in [23] and [36] that reduces the order of the state-space model and the number of inputs. The obtained reduced-order model is also convenient when one wishes to describe the MMC neglecting the discontinuities.

One can start defining the reduced model by considering the MMC model described in (3) and assuming that the capacitor voltages are balanced, i.e., we have

$$v_i^u(t) = v^u(t), \quad \forall i \in \{1, 2, \ldots, N\} \quad (10)$$

and[1]

$$v_i^l(t) = v^l(t), \quad \forall i \in \{1, 2, \ldots, N\}. \quad (11)$$

Then, the MMC model (3) reduces to

$$\dot{x}(t) = A\left(\breve{\mu}^u(t), \breve{\mu}^l(t)\right)x(t) + B[v_{\text{dc}} \quad v_{\text{ac}}^*]^T \quad (12)$$

where

$$A\left(\breve{\mu}^u(t), \breve{\mu}^l(t)\right) \triangleq$$

$$\begin{bmatrix} -\frac{R}{L} & 0 & -\frac{1}{2L}\breve{\mu}^u(t) & -\frac{1}{2L}\breve{\mu}^l(t) \\ 0 & -\frac{R+2R_l}{L+2L_l} & -\frac{1}{L+2L_l}\breve{\mu}^u(t) & \frac{1}{L+2L_l}\breve{\mu}^l(t) \\ \frac{1}{NC}\breve{\mu}^u(t) & \frac{1}{2NC}\breve{\mu}^u(t) & 0 & 0 \\ \frac{1}{NC}\breve{\mu}^l(t) & -\frac{1}{2NC}\breve{\mu}^l(t) & 0 & 0 \end{bmatrix} \quad (13)$$

$$B \triangleq \begin{bmatrix} \frac{1}{2L} & 0 & 0 & 0 \\ 0 & -\frac{2}{L+2L_l} & 0 & 0 \end{bmatrix}^T \quad (14)$$

[1]Note that $v^u(t) = v^l(t)$ is not imposed. Thus, the model allows capacitor voltages in the upper arm to be different from those in the lower arm.

and the system state is now given by

$$x(t) \triangleq \left[\, i_c(t) \; i_l(t) \; v^u(t) \; v^l(t) \,\right]^T. \quad (15)$$

In this model, the modulation functions are

$$\breve{\mu}^u(t) \triangleq \sum_{j=1}^{N} \mu_j^u(t), \quad \breve{\mu}^u(t) \in \{0, \ldots, N\} \quad (16)$$

and

$$\breve{\mu}^l(t) \triangleq \sum_{j=1}^{N} \mu_j^l(t), \quad \breve{\mu}^l(t) \in \{0, \ldots, N\}. \quad (17)$$

These functions represent the number of modules inserted in the upper and lower arms, respectively, and depend on the control law adopted.

A detailed procedure to obtain the previous expressions can be found in [23].

As stated before, the reduced-order model in (12) uses the control signals in (16) and (17). Since these aggregated control signals are the sum of the binary control signals $\mu_j^{u,l}$, they represent quantized signals that only take integer values between 0 and N.

The reduced-order model facilitates the derivation of analytical solutions by reducing the number of input variables and the size of the state vector. This can be used for a more detailed analysis of the converter such as in [23] and [36].

It is important to note that when the reduced-order model is used, it is implicitly assumed that the voltages in all the capacitors are balanced according to (10) and (11). Note that when this condition is fulfilled, it is possible to represent the capacitors of all modules with one capacitor per arm and define aggregated control signals $\mu_j^{u,l}$ without using any approximation. All the information about any modulation technique used, or about the control inputs $\mu_j^{u,l}$ in general, is now contained in $\breve{\mu}^{u,l}$ as defined in (16) and (17). Thus, if the voltages of the capacitors are balanced [see (10) and (11)], then the full-order model and the reduced-order model using $\breve{\mu}^{u,l}$ provide the same result.

IV. Application of the Reduced-Order Model

A. Implications of Using Continuous Control Signals

In some cases, it may be convenient to express the aggregated control signals in (16) and (17) as the sum of an equivalent continuous valued signal $\mu^{u,l}(t)$ and a quantization effect $Q_n(t)$, produced by having only a finite number of modules in the converter, as follows:

$$\breve{\mu}^{u,l}(t) = \mu^{u,l}(t) + Q_n(t). \quad (18)$$

If desired, $Q_n(t)$ can be neglected using only the continuous part $\mu^{u,l}(t)$. In particular, if $\mu^{u,l}(t)$ are smooth, then only differentiable functions need to be taken into account, easing the analysis. Note that this step implies an approximation and it is specially important when a low number of modules are available ($Q_n(t)$ comparable with $\mu^{u,l}(t)$). It is because of this approximation that the results of the reduced-order model may differ from the ones of the full-order MMC.

TABLE I
PARAMETER VALUES IN PER UNIT (P.U.) AT $\omega = 2\pi 50$ FOR AN MMC

Variable	R	$X_L\ (\omega L)$	$X_C\ \left(\frac{1}{\omega C}\right)$	R_l	$X_{L_l}\ (\omega L_l)$	v_{dc}	v^*_{ac}	N
Value	0.004	0.075	0.089	0.01	0.15	2.19	1	8

[The p.u. values are normalized with respect to the grid voltage (3800 V) and the nominal current (650A)].

Neglecting the quantization allows one to obtain analytical expressions of variables such as the capacitor voltages. These expressions can then be used for optimization and reference design [23]. However, the quantization affects the frequency response of the circuit, leading to inaccuracies when this is neglected.

Due to the nonlinearity in the model, there is a modulation effect that comes from the multiplication of the control signal with the capacitor voltages, see (12). This effect moves the resonant frequencies (i.e., peaks of amplitude in i_c) of the converter when additional frequency components are considered in the control signals. As shown next, this accentuates the error of the reduced-order model at some specific frequencies.

To illustrate the effect of the quantization at different frequencies, let us consider numerical values of the parameters of the converter as in Table I. Moreover, let us define the following control inputs.

1) Smooth control inputs

$$\mu^u(t) = N\frac{1+\cos(\omega t)}{2}, \quad \mu^l(t) = N\frac{1-\cos(\omega t)}{2}. \tag{19}$$

2) Quantized control inputs

$$\breve{\mu}^u(t) = \text{ni}\left(N\frac{1+\cos(\omega t)}{2}\right),$$
$$\breve{\mu}^l(t) = \text{ni}\left(N\frac{1-\cos(\omega t)}{2}\right) \tag{20}$$

where the operation ni(•) approximates the argument to the nearest integer.

Fig. 2 shows the response of an open-loop MMC to the control inputs in (19) and (20) with fundamental frequency $\omega = 2\pi 60$. A clear difference between the two cases (with and without quantization) can be observed. Interestingly, the situation changes when the frequency of the sinusoidal input is changed to $\omega = 2\pi 50$, see Fig. 3. The simulation shows that the difference between the response of the model without the quantization and the model with the quantization is minimal for this frequency. In Fig. 4, a simulation with the error produced by neglecting the quantization effect for MMCs with different number of modules is shown. The error is calculated as the root mean square (RMS) of the difference of the simulated waveforms over one period in steady state. The simulation shows that a larger error is presented for some specific frequencies. The lower the number of levels the larger this error tends to be. However, sufficiently far from the aforementioned frequencies, the error for $N = 4$, $N = 8$, and $N = 12$ becomes low and very

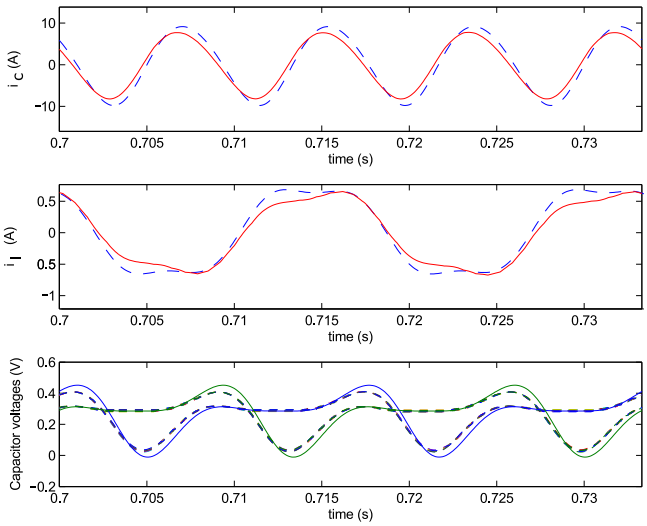

Fig. 2. Effects of the quantization at 60 Hz (Solid lines: Without quantization, dashed lines: With quantization).

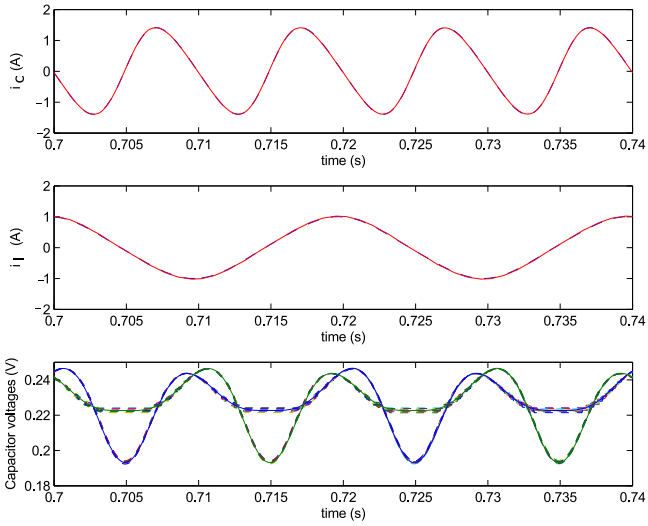

Fig. 3. Effects of the quantization at 50 Hz (Solid lines: Without quantization, dashed lines: With quantization).

similar. This also holds true for a higher number of levels, which implies that the reduced-order model represents a good approximation of the MMC even with a low number of levels as long as the operation is sufficiently far from these critical frequencies. In the following sections, the reasons behind these differences are going to be analyzed in more detail.

In Fig. 4, several peaks in the error plots can be noticed. In general, it is possible to group these peaks into two different cases: the high-frequency peak (around 60 Hz) and its duplicates due to the nonlinearities in the system (i.e., modulation due to the multiplication of the control signal an the module voltages), and the low-frequency peak (around 15 Hz) and its duplicates. In Fig. 4, this grouping is shown for the case with $N = 8$. These error peaks are directly related with the resonant frequencies of the converter. We shall give special attention to the peak with the highest frequency since it may be located close to the typical

$$\dot{i_c}(t) = -\frac{R}{L}i_c(t) - \frac{1}{2L}\left(1-\beta^u \mathrm{u}\left(-i_c-\frac{i_l}{2}\right)\right)\left(N\beta^u + \breve{\mu}^u(t)\left(1-\beta^u\right)\right)v^u$$
$$-\frac{1}{2L}\left(1-\beta^l \mathrm{u}\left(-i_c+\frac{i_l}{2}\right)\right)\left(N\beta^l + \breve{\mu}^u(t)\left(1-\beta^l\right)\right)v^l + \frac{1}{2L}v_{\mathrm{dc}} \tag{21}$$

$$\dot{i_l}(t) = -\frac{R+2R_l}{L+2L_l}i_l(t) - \frac{1}{L+2L_l}\left(1-\beta^u \mathrm{u}\left(-i_c-\frac{i_l}{2}\right)\right)\left(N\beta^u + \breve{\mu}^u(t)\left(1-\beta^u\right)\right)v^u$$
$$+\frac{1}{L+2L_l}\left(1-\beta^l \mathrm{u}\left(-i_c+\frac{i_l}{2}\right)\right)\left(N\beta^l + \breve{\mu}^u(t)\left(1-\beta^l\right)\right)v^l - \frac{2}{L+2L_l}v^*_{\mathrm{ac}} \tag{22}$$

$$\dot{v}^u(t) = \left(\frac{1}{NC}i_c + \frac{1}{2NC}i_l\right)\left(N\beta^u + \breve{\mu}^u(t)\left(1-\beta^u\right)\right)\left(1-\beta^u \mathrm{u}\left(-i_c-\frac{i_l}{2}\right)\right) \tag{23}$$

$$\dot{v}^l(t) = \left(\frac{1}{NC}i_c - \frac{1}{2NC}i_l\right)\left(N\beta^l + \breve{\mu}^l(t)\left(1-\beta^l\right)\right)\left(1-\beta^l \mathrm{u}\left(-i_c+\frac{i_l}{2}\right)\right) \tag{24}$$

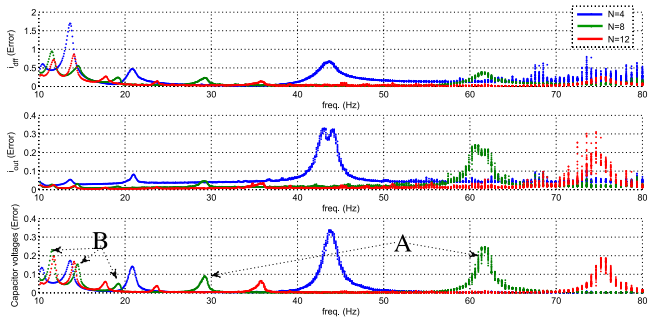

Fig. 4. Error produced by the quantization effect using 4, 8, and 12 modules for different frequency values. (A) High frequency peaks. (B) Low frequency peaks.

operating frequencies of the converter (50 Hz or 60 Hz). This observation shows that the quality of the model is frequency dependent and motivates our subsequent analysis.

Let us fist define what we shall refer to as the "frequency response of the MMC." Due to the nonlinear nature of the system, frequencies multiples of the input frequency are likely to appear in the converter currents and voltages. This motivates us to define the frequency response of the MMC as the amplitude of the second harmonic of the circulating current i_c as a function of the frequency in the control signals ω [see (19) and (20)]. The reason why the second harmonic of i_c is chosen for the analysis is mainly due to the following facts:

1) this is the lowest order harmonic in the circulating current;
2) its amplitude is significantly higher than the amplitude of the other harmonics;
3) as shown in Fig. 4, the resonance of this second-order harmonic is more likely to match the operating frequency of the converter.[2]

In the following sections, we are going to focus our efforts into determining the relation of these resonant frequencies with the converter parameters.

[2]Note that the resonant frequencies are independent of our choice of considering the second-order harmonic of i_c as output variable for the analysis.

B. Effects of Capacitor Voltage Imbalances in the Reduced-Order Model

The reduced-order model assumes that the capacitor voltages in all the modules are properly balanced. If this holds true, the prediction of the reduced-order model can closely match its full-order counterpart, as shown in Fig. 3. However, good voltage balancing is not always possible.

This section aims to evaluate the effects of module voltage imbalances in the accuracy of the reduced-order model. This analysis is done by setting a voltage balancing control algorithm in the full-order MMC that allows an specific maximum voltage difference between the modules of the same arm, also known as voltage imbalance ($\delta v^{u,l}_{\max}$). This result is then compared with the prediction of the reduced-order model for several values of $\delta v^{u,l}_{\max}$.

In Fig. 5, the increment of the RMS error of the reduced-order model as a function of the relation between the maximum allowed voltage imbalance $\delta v^{u,l}_{\max}$ and the module voltage ripple $\Delta v^{u,l}$ is shown. For this test, a frequency of 50 Hz is used and the reference RMS error values are taken from Fig. 4 ($N = 8$). As expected, the error presented in the module voltages is increased significantly due to the allowed imbalance. However, for the rest of the variables, an increment of less than 10%, with an allowed voltage imbalance of up to 35% of the module voltage ripple, is shown. It is worth noticing that the circulating current is more affected by the voltage imbalances due to the low arm impedance.

C. Inclusion of the Blocking Deblocking Modes

As protective measure, the blocking mode is commonly used in unbalanced grid conditions. This mode consists in switching off all the semiconductors in the modules on either of the arms of the converter, forcing the current to flow through the parallel diode associated to the semiconductor devices. In order to include the blocking mode in the simplified model of the MMC, the equivalent configuration shown in Fig. 6 can be used. More details of this configuration and blocking and deblocking modes can be found in [37] and [38], where the configuration in Fig. 6 was originally proposed.

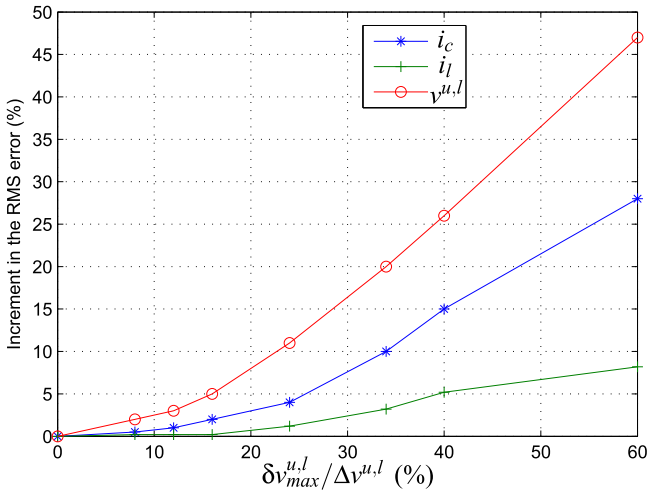

Fig. 5. Increment in the RMS error of the prediction of the reduced-order model introduced by voltage imbalances in the capacitors as a function of the relation between the maximum voltage difference between capacitors of the same arm (voltage imbalance $\delta v^{u,l}_{\max}$) and the voltage ripple $\Delta v^{u,l}$. Reference values: $i_c(\text{error}) = 8.3 \cdot 10^{-3}$, $i_l(\text{error}) = 17.7 \cdot 10^{-3}$, $i_c(\text{error}) = 4 \cdot 10^{-3}$, and $\Delta v^{u,l} = 0.05$ p.u.

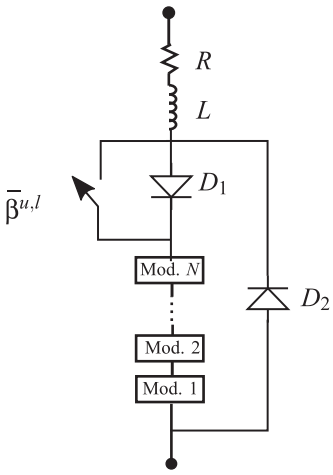

Fig. 6. MMC arm including blocking and deblocking modes. In blocking mode ($\beta^{u,l} = 1$ switch open), D_1 blocks partially the current that goes through the modules. In this case, the current flows through D_2 instead. In blocking mode $\mu^{u,l}$ are set to N.

The original MMC equations in (12) can be modified to include the blocking modes as follows: where $\mathrm{u}(*)$ represents the step function, and β^u and β^l represent the blocking signals of the upper and lower arm, respectively ($\beta^{u,l} = 1$ represents a blocked arm). In this state the control signals $\mu^{u,l}$ are forced to N and the arm voltage depends on the direction of the current (see Fig. 6).

In the following sections, the frequency response of the MMC will be analyzed. However, due to the mathematical complexity that arises when the blocking mode is included [see (21)–(24)] as shown at the top of the perious page, the method presented in Section VI used to analyze the frequency response cannot be applied due to the impossibility of transforming the system into a component wise linear system as in (32). For this reason, the frequency analysis is going to be performed without including the blocking mode [see (12)].

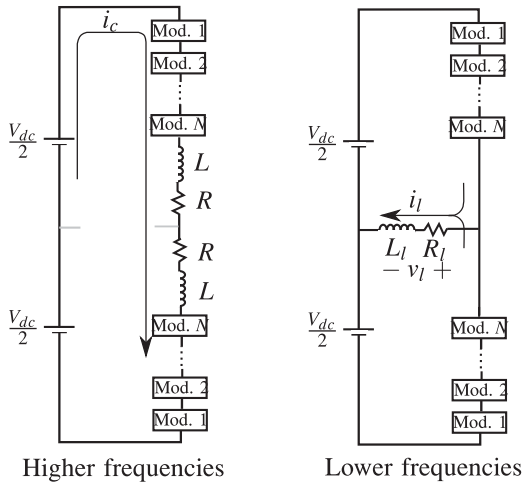

Fig. 7. Approximate circuits of the MMC to compute its resonant frequencies.

V. Estimation of the MMC Frequency Response (Linearization Approach)

This section presents a preliminary approach to obtain information about the frequency response of the MMC that uses a linearized version of the reduced-order model around an operation point. The linearization technique is widely used in many applications. One of them is the design of control laws for power converters, where it is important that the information provided by the linearized model matches as close as possible the original model to guarantee proper performance and good stability properties. This approach aims to derive simple analytical expressions for the resonant frequencies based on linear differential equations that will later be used for comparison with more elaborated approaches. This will also serve as a criteria to determine the accuracy of the linearized model of the MMC.

The linear model (12) can be written, based in (12), as follows:

$$\dot{\tilde{x}}(t) = A\left(\bar{\mu}^u, \bar{\mu}^l\right)\tilde{x}(t) + B(x(0))[v_{\text{dc}} \quad v^*_{\text{ac}} \quad \tilde{\mu}^{u,l}(t)]^T \quad (25)$$

where $\bar{\mu}^{u,l}$ represent the control signals in the operational point $\tilde{\mu}^{u,l}(t)$ and $\tilde{x}(t) = [\tilde{i}_c \quad \tilde{i}_l \quad \tilde{v}^u \quad \tilde{v}^l]$ represent the incremental variables associated with the control signals and the state-space vector, respectively, and $B(x(0))$ represent a constant matrix that depends on the initial conditions $x(0)$. Since the matrix $A\left(\bar{\mu}^u, \bar{\mu}^l\right)$ is in charge of determining the placement of the poles and resonant frequencies of the system, we focus our analysis in this term of the equation.

To simplify the calculations, let us assume that $\|R + j\omega L\| \ll \|R_l + j\omega L_l\|$. Therefore, the resonant frequencies can be analyzed by considering two different circuits of the MMC: A circuit for the higher frequencies and an additional circuit for the lower frequencies, as it is shown in Fig. 7.

The following analysis uses this assumption and the linearized model in (25) to derive analytical expressions of the resonant frequencies of the MMC. In Section VI, the results of the resonant frequencies obtained with the linearized model will be compared with results obtained with more accurate methods, which can be very useful when one wish to evaluate the accuracy of the linearized model specially in the case of stability of

control loops. Moreover, it will provide more insight into the problem explaining the results in Fig. 4.

A. High Frequencies

Under the assumptions $\|R + j\omega L\| \ll \|R_l + j\omega L_l\|$, it is possible to write the differential equations of the linear system in (25), and taking into account that the operation lies in the high frequency range, as shown in Fig. 7 (i.e., $\|R_l + j\omega L_l\| \to \infty$ or $i_l = 0$), develop analytical expressions for the resonant frequencies of the converter. According to (25), the following holds:

$$\dot{\tilde{i}}_c = -\frac{R}{L}\tilde{i}_c - \frac{1}{2L}\bar{\mu}^u\tilde{v}^u - \frac{1}{2L}\bar{\mu}^l\tilde{v}^l + \cdots$$
$$\dot{\tilde{v}}^u = \frac{1}{NC}\bar{\mu}^u\tilde{i}_c + \cdots \qquad \dot{\tilde{v}}^l = \frac{1}{NC}\bar{\mu}^l\tilde{i}_c + \cdots . \tag{26}$$

For the sake of simplicity, some terms are omitted in (26) since they have no effect over the value of the resonant frequencies.

By obtaining the second derivative of $\tilde{i}_c$ using (26), and substituting $\dot{\tilde{v}}^u$ and $\dot{\tilde{v}}^l$, the following is obtained:

$$\ddot{\tilde{i}}_c = -\frac{R}{L}\dot{\tilde{i}}_c - \frac{1}{2L}\bar{\mu}^u\left(\frac{1}{CN}\bar{\mu}^u\right)\tilde{i}_c - \frac{1}{2L}\bar{\mu}^l\left(\frac{1}{CN}\bar{\mu}^l\right)\tilde{i}_c + \cdots$$
$$= -\frac{R}{L}\dot{\tilde{i}}_c - \frac{1}{2LCN}\left((\bar{\mu}^u)^2 + (\bar{\mu}^l)^2\right)\tilde{i}_c + \cdots . \tag{27}$$

It is assumed that $\bar{\mu}^u + \bar{\mu}^l = N$ and $\bar{\mu}^u = \alpha N$, where $0 < \alpha < 1$. α is a constant value that depends on the linearization point. Using the second-order differential equation in (27), a value for the resonant frequency can be obtained as follows:

$$f_1 = \frac{1}{\sqrt{\frac{2LC}{N}\frac{1}{\alpha^2+(1-\alpha)^2}}}, \quad \frac{\sqrt{2}}{2}\frac{1}{\sqrt{\frac{2LC}{N}}} \le f_1 < \frac{1}{\sqrt{\frac{2LC}{N}}}. \tag{28}$$

Due to the fact that i_c contains mainly second-order harmonic, an interesting phenomenon occurs. This consists in the resonance being produced when the input frequency is equals to $\frac{f_1}{2}$. Due to the system nonlinearities, this input frequency produces an i_c with frequency f_1, matching the resonance frequency. Note that this phenomenon is not captured by the linear model analyzed in this section. This will be corroborated and analyzed further with the method presented in Section VI.

B. Low Frequencies

For the low-frequency case, as shown in Fig. 7, R and L are considered as 0. Equation (25) can be used under this consideration to write the following set of differential equations:

$$0 = -\bar{\mu}^u\tilde{v}^u - \bar{\mu}^l\tilde{v}^l + \cdots ,$$
$$\dot{\tilde{i}}_l = -\frac{R_l}{L_l}\tilde{i}_l - \frac{1}{2L_l}\bar{\mu}^u\tilde{v}^u + \frac{1}{2L_l}\bar{\mu}^l\tilde{v}^l + \cdots$$
$$\dot{\tilde{v}}^u = \frac{1}{NC}\bar{\mu}^u\left(\tilde{i}_c + \frac{\tilde{i}_l}{2}\right) + \cdots ,$$
$$\dot{\tilde{v}}^l = \frac{1}{NC}\bar{\mu}^l\left(\tilde{i}_c - \frac{\tilde{i}_l}{2}\right) + \cdots . \tag{29}$$

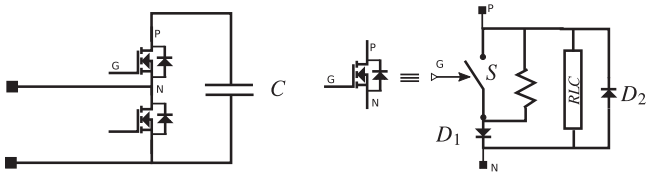

Fig. 8. Detailed model of the MMC module including the detailed model of the semiconductor switches used in PSCAD/EMTDC. The model of the semiconductor switch includes an ideal switch S, a snubber RLC circuit, and two nonlinear diodes D_1 and D_2.

In an analogous procedure as for the high-frequency case, the second derivative of $\tilde{i}_l$ is obtained and $\dot{\tilde{v}}^u$ and $\dot{\tilde{v}}^l$ are substituted, leading to

$$\ddot{\tilde{i}}_l = -\frac{R_l}{L_l}\dot{\tilde{i}}_l + \frac{1}{L_l}\bar{\mu}^l\dot{\tilde{v}}^l$$
$$= -\frac{R_l}{L_l}\dot{\tilde{i}}_l - \frac{1}{NL_lC}\frac{1}{\left(\frac{1}{\bar{\mu}^u}\right)^2 + \left(\frac{1}{\bar{\mu}^l}\right)^2}\tilde{i}_l + \cdots . \tag{30}$$

Considering again that $\bar{\mu}^u + \bar{\mu}^l = N$ and $\bar{\mu}^u = \alpha N$, where $0 < \alpha < 1$, and using the second-order differential equation in (30), a value for the resonant frequency can be obtained as follows:

$$f_2 = \frac{1}{\sqrt{\frac{L_lC}{N}\left(\frac{\alpha^2+(1-\alpha)^2}{\alpha^2(1-\alpha)^2}\right)}}, \quad 0 < f_2 \le \frac{\sqrt{2}}{4}\frac{1}{\sqrt{\frac{L_lC}{N}}}. \tag{31}$$

VI. Estimation of the Frequency Response of the MMC (Fourier Approach)

In order to address the problem of obtaining information about the frequency response of the MMC in more detail, an approach using Fourier-series approximation that analyzes each frequency component separately is applied. For detailed information of such techniques please refer to [39] and [40]. In [41] and [42], this Fourier method is applied to an MMC under nominal operating conditions and validated against a fully detailed electromagnetic transient model in PSCAD/EMTDC (see Fig. 8). In the previously mentioned works, each of the semiconductor switches used in the converter modules are modeled using an ideal switch S, diodes D_1 and D_2 in series and antiparallel configurations, which are modeled using the classical diode exponential function, and a snubber circuit. This model has been used successfully in studies for large-scale implementations showing a good representation of its real-life counterpart. More details on this model and its application can be found in [43].

The results in [41] and [42] show good accuracy of the Fourier-series approximation with as low as two harmonic components. Moreover, it is also shown that by increasing the harmonic components up to 17, the results are considerably improved, obtaining a very close match between the model in PSCAD/EMTDC and the approach using Fourier series. Therefore, we shall consider the model presented in this section can be considered as a good reference for the accuracy assessment of the reduced-order model.

Using the Fourier-series approximation, the MMC can be described by the following equation:

$$\mathbf{M}(\omega)\mathbf{z} = \mathbf{U} \tag{32}$$

where (33) is shown at the bottom of this page

$$\mathbf{U} \triangleq \begin{bmatrix} -\frac{1}{2}\mathbf{V_{in}} & 0 & 0 & 0 \\ 0 & \frac{2L_l}{L+2L_l}\mathbf{V}^*_{\mathbf{ac}} & 0 & 0 \end{bmatrix}^T \tag{34}$$

and

$$\mathbf{z} \triangleq \begin{bmatrix} \mathbf{I_c} & \mathbf{I_l} & \mathbf{V^u} & \mathbf{V^l} \end{bmatrix}^T \tag{35}$$

are matrices constructed based on the Fourier transformation of (12). The diagonal matrix $\mathbf{n}$ is defined as follows:

$$\mathbf{n} \triangleq \quad \text{diag}\left(\begin{bmatrix} -n & -(n-1) & \cdots & 0 & \cdots & n-1 & n \end{bmatrix}\right) \tag{36}$$

where n is the number of frequency components used in the Fourier-series expansion.

The variables $\mathbf{V_{in}}$, $\mathbf{V}^*_{\mathbf{ac}}$, $\mathbf{I_c}$, $\mathbf{I_l}$, $\mathbf{V^u}$, and $\mathbf{V^l}$ are vectors that contain each of the coefficients of the Fourier-series expansion of the respective variable. As an example, let us assume that $i_c(t)$ can be written as follows:

$$i_c(t) = \sum_{k=-n}^{n} i_c^{(k)} e^{j\omega n t}. \tag{37}$$

With this, the variable $\mathbf{I_c}$ can be defined as follows:

$$\mathbf{I_c} \triangleq \begin{bmatrix} i_c^{(-n)} & \cdots & i_c^{(0)} & \cdots & i_c^{(n)} \end{bmatrix}^T. \tag{38}$$

where $i_c^{(j)}$ represent the coefficient corresponding to the jth multiple of the natural frequency of i_c.

The matrices $\mathbf{Y_j}$ represent the Fourier decomposition of the control inputs and are defined as follows:

$$\mathbf{Y_j} \triangleq \begin{bmatrix} Y_j^{(0)} & \cdots & Y_j^{(-2n)} \\ & \ddots & \\ \vdots & Y_j^{(0)} & \vdots \\ & \ddots & \\ Y_j^{(2n)} & \cdots & Y_j^{(0)} \end{bmatrix} \tag{39}$$

where $Y_j^{(k)}$ represent the coefficient corresponding to the kth multiple of the natural frequency of the control signals μ^j.

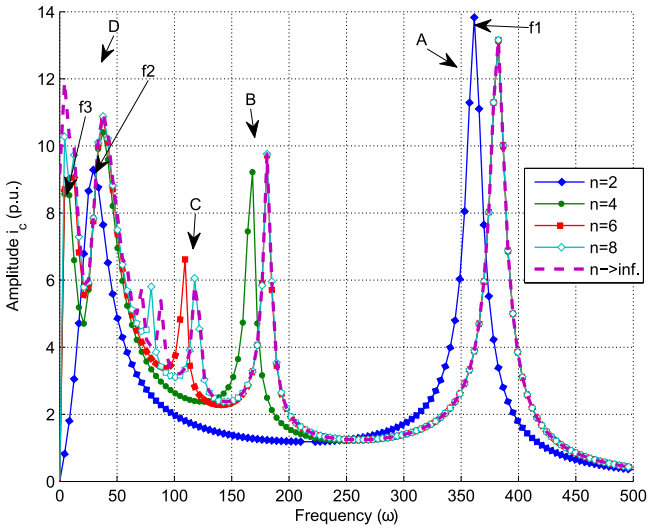

Fig. 9. Estimation of the amplitude of i_c using the Fourier-series approximation for different values of n.

With the previous definitions, the vector $\mathbf{z}$ can be found using the following expression [see (32)]:

$$\mathbf{z} = (\mathbf{M}(\omega))^{-1}\mathbf{U}. \tag{40}$$

Since the system described by (32) is linear, it is possible to find the resonant frequencies of the system by solving ω by the following equation:

$$\det(\mathbf{M}(\omega)) = 0. \tag{41}$$

In order to illustrate the results of this method, Fig. 9 shows the frequency response of i_c for different numbers of frequency components n. It can be seen that the resonant frequencies move and some new ones appear when the value of n is increased. In particular, the peaks marked as "A" correspond to the resonance of the second harmonic of i_c, "B" to the resonance of the fourth harmonic, "C" to the resonance of the sixth harmonic, and "D" to the resonances dominated by the load impedance.

It is possible to obtain analytical expressions for some of the resonant frequencies in terms of the converter components. This can be done by solving (41) for a given value of n. For the sake of simplicity, only the continuous control signals in (19) are going to be considered for this analysis.

$$\mathbf{M}(\omega) \triangleq \begin{bmatrix} -(R\mathbf{I} + j\omega\mathbf{n}L) & 0 & -\frac{1}{2}\mathbf{Y_u} & -\frac{1}{2}\mathbf{Y_l} \\ 0 & -\left(\frac{R+2R_l}{L+2L_l}\mathbf{I} + j\omega\mathbf{n}L_l\right) & -\frac{L_l}{L+2L_l}\mathbf{Y_u} & \frac{1}{L+2L_l}\mathbf{Y_l} \\ \frac{1}{NC}\mathbf{Y_u} & \frac{1}{2NC}\mathbf{Y_u} & -j\omega\mathbf{n}C & 0 \\ \frac{1}{NC}\mathbf{Y_l} & -\frac{1}{2NC}\mathbf{Y_l} & 0 & -j\omega\mathbf{n}C \end{bmatrix} \tag{33}$$

TABLE II
COMPARISON OF THE RESONANT FREQUENCIES f_1 AND f_2 (SEE FIG. 9) OBTAINED WITH DIFFERENT METHODS FOR $n = 2$: ACTUAL: USING (41) WITH $n \to \infty$ AND QUANTIZED CONTROL SIGNALS

	Actual	Fourier (Num.)	Fourier (Ana.)	Lin.
f_1	382.6	361.4	362.4	582.4–823.7
f_2	50.4	29.3	28.3	0–265.5

Fourier (Num.): Using (41) with $n = 2$ and continuous control signals. Fourier (Ana.): Using (42) and (43). Lin.: Using (28) and (31).

Note that the frequency response may change, if the amplitude or characteristics of these control signals change due to the nonlinear properties of the system.

The results of the analysis of the frequency response using the Fourier series are shown in the sections ahead. For some numerical comparisons, the values of Table I are used.

A. Frequency Response Analysis With $n = 2$

In order to begin with the analysis, matrices $\mathbf{n}$, $\mathbf{Y_u}$, $\mathbf{Y_l}$, and $\mathbf{U}$ in (14), (36), and (39), respectively, need to be defined using $n = 2$ and the control signals in (19). These matrices can be used to define $M(\omega)$ [see (33)] and then to obtain the solution $\mathbf{z}$ by applying (40). Consequently, the resonant frequencies can be obtained using (41).

After some algebraic manipulations, the following simplified expressions for the frequencies f_1 and f_2 in Fig. 9 can be derived:

$$f_1 = \left(\frac{28CL^2R^2 + 80CL^2RR_l + 64CL^2R_l^2}{32CL^2(L^2 + 4LL_l + 4L_l^2)} - \frac{16CLL_lR^2 + 16CL_l^2R^2 - 8L^3N - 22L^2L_lN - 12LL_l^2N}{32CL^2(L^2 + 4LL_l + 4L_l^2)} \right)^{\frac{1}{2}}, \tag{42}$$

$$f_2 = \mathrm{Re}\left(\sqrt{\frac{L_lN - 32CR_l^2 + 8\sqrt{16C^2R_l^4 - CL_lNR_l^2}}{64L_l^2C}} \right). \tag{43}$$

where $\mathrm{Re}(*)$ represents the real part of the argument. Table II shows a comparison of the numerical values of the resonant frequencies obtained with different methods. It can be seen that the analytical expressions [see (42) and (43)] approximate the numerical results with an error less than 4%. The approach based on linearization in Section V gives a very easy method to compute these values; however, the accuracy of the result is compromised. Note that the phenomenon mentioned in Section V where the resonance due to f_1 is produced when the input is at $\frac{f_1}{2}$ can be seen clearly in this comparison. The linearized approach fails to model this phenomenon producing values for f_1 that are around twice as high as the actual value. Remember also that f_1 is of special importance since it could match the operating frequency of the converter and thereby producing inaccuracies in the reduced-order model.

TABLE III
COMPARISON OF THE RESONANT FREQUENCIES f_3 (SEE FIG. 9) OBTAINED WITH DIFFERENT METHODS FOR $n = 4$: ((ACTUAL: USING (41) WITH $n \to \infty$ AND QUANTIZED CONTROL SIGNALS))

	Actual	Fourier (Num.)	Fourier (Ana.)
f_3	4.2	8.4	7.88

Fourier (Num.): Using (41) with $n = 4$ and continuous control signals. Fourier (Ana.): Using (44).

B. Frequency Response Analysis With $n \geqslant 4$

The complexity of the expressions obtained by solving (40) grows exponentially with n. For $n = 4$, it is possible to obtain relatively simple analytical expressions only for f_3 (see Fig. 9). After some algebraic manipulations, the expression for f_3 can be written as follows:

$$f_3 = \mathrm{Re}\left(N \left(5\frac{23712CR_l^2 - 127L_lN}{177209344R_l^4C^3} - \frac{\sqrt{559490048C^2R_l^4 - 6022848CL_lNR_l^2 + 16129L_l^2N^2}}{177209344R_l^4C^3} \right)^{\frac{1}{2}} \right). \tag{44}$$

As in the case with $n = 2$, this expression is a simplified version of the solution. Table III shows a comparison of the numerical values obtained with different methods.

For the remaining resonant frequencies, no simple closed form expression could be obtained for $n = 4$. Therefore, the solutions are computed numerically. This also applies to the cases with $n > 4$. Fig. 9 shows the numerical values for the most important frequencies for different values of n. It is possible to see that, the more terms are used in the Fourier approximation, the more resonant frequencies appear and some others change their position.

C. Effects of the Quantization $Q_n(t)$ of the Control Signals

Due to the nonlinear nature of the system, the inclusion of the quantization changes the frequency response of the system. To take this effect into account, the control signals in (20) are used for the following analysis.

Fig. 10 shows a comparison of the frequency response of the reduced-order model calculated with the Fourier approximation for $n = 2$ with and without the quantization. It can be seen how the resonant frequencies change their position and the amplitudes of the peaks are slightly attenuated. Unfortunately, it is not possible to obtain analytical expression for the resonant frequencies when the quantization is taken into account for $n \geq 2$ due to the complexity of the expressions. However, they can be obtained numerically by solving (41).

Fig. 11 shows the results for $n = 6$. For this case, the resonant frequencies are also affected by the quantization; especially, the amplitude corresponding to the resonance of the fourth harmonic (frequency peak between 150 rad/s and 200 rad/s) is attenuated significantly once the quantization is taken into account. Moreover, the resonant frequency with the highest value is displaced

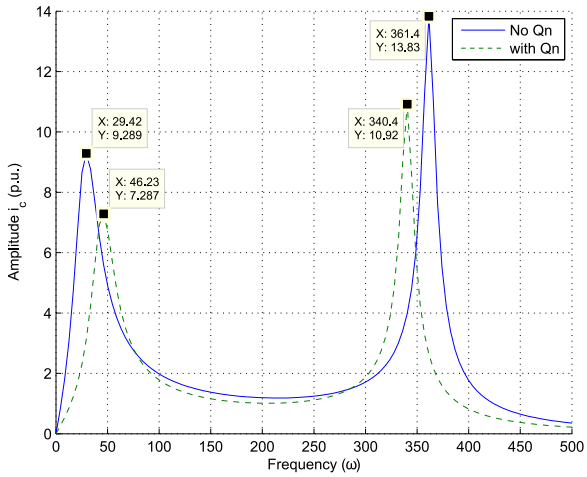

Fig. 10. Frequency response of the MMC for $n = 2$ with and without quantization.

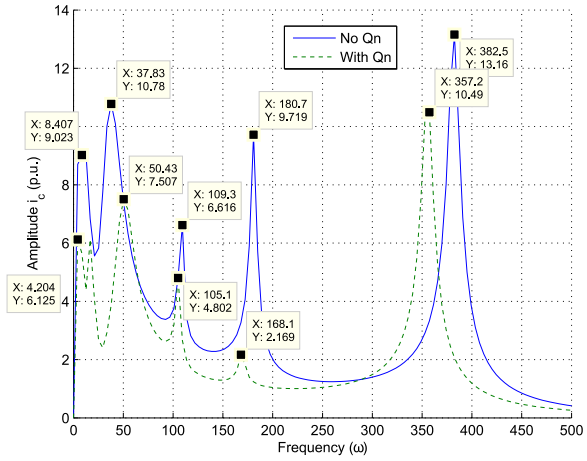

Fig. 11. Frequency response of the MMC for $n = 6$ with and without quantization.

around 7% due to the quantization. This displacement in frequency is less pronounced for the other resonant frequencies.

The difference of the two frequency responses in Fig. 11 corresponds to the error caused by neglecting the quantization. Since the amplitude peaks are at slightly different locations, the difference between the two frequency responses becomes significantly close to them. This explains the peaks obtained in the simulation already shown in Fig. 4, where the error of the model without quantization was illustrated.

VII. Conclusion

A reduced-order model can accurately represent the behavior of the MMC in many situations. However, aspects as voltage imbalances and quantization can affect its accuracy. This paper analyzes the impact of both of these aspects on the accuracy of the reduced-order model showing the relation between voltage imbalances and the increment of its prediction error. Moreover, the effect of the quantization in the control signals for different operation frequencies is also addressed. The current manuscript has extensively analyzed the inaccuracy introduced by the quantization effect as a function of the frequency of operation showing that in frequency ranges close to the resonant frequencies, the accuracy of the reduced-order model is reduced.

This paper has developed detailed methods to characterize resonant frequencies of MMC's by using analytical expressions. This novel analysis allows one to obtain values of the resonant frequencies that have not been identified in the current literature, giving additional insight on the MMC. The results obtained here can be used to estimate beforehand if the reduced-order model produces an accurate representation of the MMC, and the insight gained is particularly useful when working with control techniques using continuous control signals. The presented approach based on a linearized model also serves as a good starting point for evaluating the accuracy of the linearization of the MMC giving insight in how to proceed when designing any control law. The fact that the linear model fails to represent complex behavior results in an estimation of the frequency f_1 that can be twice as high as the real resonant frequency.

For the sake of accuracy, working close to any of the resonant frequencies of the converter should be avoided. This becomes more important the lower the number of levels used, since here the amplitude of the quantization grows in relation with the continuous approximation of the control signals. It is also shown that the reduced-order model produces the same results as the full-order MMC when the quantization is taken into account. Therefore, when using control techniques with quantized variables such as finite control set MPC [44], the accuracy problem becomes less significant.

References

[1] A. Lesnicar and R. Marquardt, "An innovative modular multilevel converter topology suitable for a wide power range," in *Proc. IEEE Bologna Power Tech Conf.*, Jun. 2003, vol. 3, pp. 1–6.

[2] M. Malinowski, K. Gopakumar, J. Rodriguez, and M. Perez, "A survey on cascaded multilevel inverters," *IEEE Trans. Ind. Electron.*, vol. 57, no. 7, pp. 2197–2206, Jul. 2010.

[3] M. Perez, S. Bernet, J. Rodriguez, S. Kouro, and R. Lizana, "Circuit topologies, modeling, control schemes, and applications of modular multilevel converters," *IEEE Trans. Power Electron.*, vol. 30, no. 1, pp. 4–17, Jan. 2015.

[4] K. Ilves, A. Antonopoulos, S. Norrga, and H.-P. Nee, "A new modulation method for the modular multilevel converter allowing fundamental switching frequency," *IEEE Trans. Power Electron.*, vol. 27, no. 8, pp. 3482–3494, Aug. 2012.

[5] M. Huang, J. Zou, and X. Ma, "An improved phase-shifted carrier modulation for modular multilevel converter to suppress the influence of fluctuation of capacitor voltage," *IEEE Trans. Power Electron.*, vol. 31, no. 10, pp. 7404–7416, Oct. 2016.

[6] S. Lu, L. Yuan, K. Li, and Z. Zhao, "An improved phase-shifted carrier modulation scheme for hybrid modular multilevel converter," *IEEE Trans. Power Electron.*, vol. 32, no. 1, pp. 81–97, Jan. 2017.

[7] S. Fan, K. Zhang, J. Xiong, and Y. Xue, "An improved control system for modular multilevel converters with new modulation strategy and voltage balancing control," *IEEE Trans. Power Electron.*, vol. 30, no. 1, pp. 358–371, Jan. 2015.

[8] K. Ilves, A. Antonopoulos, L. Harnefors, S. Norrga, L. Angquist, and H.-P. Nee, "Capacitor voltage ripple shaping in modular multilevel converters allowing for operating region extension," in *Proc. 37th Annu. Conf. IEEE Ind. Electron. Soc.*, 2011, pp. 4403–4408.

[9] R. Picas, J. Pou, S. Ceballos, J. Zaragoza, G. Konstantinou, and V. Agelidis, "Optimal injection of harmonics in circulating currents of modular multilevel converters for capacitor voltage ripple minimization," in *Proc. Energy Convers. Congr. Expo. Asia Downunder*, Jun. 2013, pp. 318–324.

[10] J. Qin and M. Saeedifard, "Predictive control of a modular multilevel converter for a back-to-back HVdc system," *IEEE Trans. Power Del.*, vol. 27, no. 3, pp. 1538–1547, Jul. 2012.

[11] B. Riar, T. Geyer, and U. Madawala, "Model predictive direct current control of modular multilevel converters: Modeling, analysis, and experimental evaluation," *IEEE Trans. Power Electron.*, vol. 30, no. 1, pp. 431–439, Jan. 2015.
[12] M. Perez, J. Rodriguez, E. Fuentes, and F. Kammerer, "Predictive control of ac-ac modular multilevel converters," *IEEE Trans. Ind. Electron.*, vol. 59, no. 7, pp. 2832–2839, Jul. 2012.
[13] Z. Gong, P. Dai, X. Yuan, X. Wu, and G. Guo, "Design and experimental evaluation of fast model predictive control for modular multilevel converters," *IEEE Trans. Ind. Electron.*, vol. 63, no. 6, pp. 3845–3856, Jun. 2016.
[14] J. Xu, P. Zhao, and C. Zhao, "Reliability analysis and redundancy configuration of MMC with hybrid submodule topologies," *IEEE Trans. Power Electron.*, vol. 31, no. 4, pp. 2720–2729, Apr. 2016.
[15] D. Wu and L. Peng, "Analysis and suppressing method for the output voltage harmonics of modular multilevel converter," *IEEE Trans. Power Electron.*, vol. 31, no. 7, pp. 4755–4765, Jul. 2016.
[16] K. Sharifabadi, L. Harnefors, H.-P. Nee, R. Teodorescu, and S. Norrga, *Design, Control and Application of Modular Multilevel Converters for HVDC Transmission Systems*. Hoboken, NJ, USA: Wiley, 2016.
[17] J. Peralta, H. Saad, S. Dennetiere, J. Mahseredjian, and S. Nguefeu, "Detailed and averaged models for a 401-level MMC-HVdc system," *IEEE Trans. Power Del.*, vol. 27, no. 3, pp. 1501–1508, Jul. 2012.
[18] J. Xu, A. M. Gole, and C. Zhao, "The use of averaged-value model of modular multilevel converter in DC grid," *IEEE Trans. Power Del.*, vol. 30, no. 2, pp. 519–528, Apr. 2015.
[19] U. Gnanarathna, A. Gole, and R. Jayasinghe, "Efficient modeling of modular multilevel HVdc converters (MMC) on electromagnetic transient simulation programs," *IEEE Trans. Power Del.*, vol. 26, no. 1, pp. 316–324, Jan. 2011.
[20] A. Beddard, C. Sheridan, M. Barnes, and T. Green, "Improved accuracy average value models of modular multilevel converters," *IEEE Trans. Power Del.*, vol. 31, no. 5, pp. 2260–2269, Oct. 2016.
[21] S. Rodrigues, A. Papadopoulos, E. Kontos, T. Todorcevic, and P. Bauer, "Steady-state loss model of half-bridge modular multilevel converters," *IEEE Trans. Ind. Appl.*, vol. 52, no. 3, pp. 2415–2425, May 2016.
[22] Q. Song, W. Liu, X. Li, H. Rao, S. Xu, and L. Li, "A steady-state analysis method for a modular multilevel converter," *IEEE Trans. Power Electron.*, vol. 28, no. 8, pp. 3702–3713, Aug. 2013.
[23] A. Lopez, D. E. Quevedo, R. P. Aguilera, T. Geyer, and N. Oikonomou, "Reference design for predictive control of modular multilevel converters," in *Proc. Aust. Control Conf.*, 2014, pp. 239–244.
[24] S. Rohner, J. Weber, and S. Bernet, "Continuous model of modular multilevel converter with experimental verification," in *Proc. IEEE Energy Convers. Congr. Expo.*, 2011, pp. 4021–4028.
[25] N. Ahmed, L. Angquist, S. Norrga, A. Antonopoulos, L. Harnefors, and H.-P. Nee, "A computationally efficient continuous model for the modular multilevel converter," *IEEE J. Emerg. Sel. Topics Power Electron.*, vol. 2, no. 4, pp. 1139–1148, Dec. 2014.
[26] H. Yang, Y. Dong, W. LI, and X. HE, "Average-value model of modular multilevel converters considering capacitor voltage ripple," *IEEE Trans. Power Del.*, vol. 32, no. 2, pp. 723–732, Apr. 2017.
[27] L. Harnefors, A. Antonopoulos, S. Norrga, L. Angquist, and H.-P. Nee, "Dynamic analysis of modular multilevel converters," *IEEE Trans. Ind. Electron.*, vol. 60, no. 7, pp. 2526–2537, Jul. 2013.
[28] L. Angquist, A. Antonopoulos, D. Siemaszko, K. Ilves, M. Vasiladiotis, and H.-P. Nee, "Open-loop control of modular multilevel converters using estimation of stored energy," *IEEE Trans. Ind. Appl.*, vol. 47, no. 6, pp. 2516–2524, Nov./Dec. 2011.
[29] A. Antonopoulos, L. Ängquist, L. Harnefors, K. Ilves, and H.-P. Nee, "Global asymptotic stability of modular multilevel converters," *IEEE Trans. Ind. Electron.*, vol. 61, no. 2, pp. 603–612, Feb. 2014.
[30] A. Jamshidifar and D. Jovcic, "Small-signal dynamic DQ model of modular multilevel converter for system studies," *IEEE Trans. Power Del.*, vol. 31, no. 1, pp. 191–199, Feb. 2016.
[31] K. Ilves, A. Antonopoulos, S. Norrga, and H.-P. Nee, "Steady-state analysis of interaction between harmonic components of arm and line quantities of modular multilevel converters," *IEEE Trans. Power Electron.*, vol. 27, no. 1, pp. 57–68, Jan. 2012.
[32] T. LI, A. M. Gole, and C. Zhao, "Harmonic instability in MMC-HVdc converters resulting from internal dynamics," *IEEE Trans. Power Del.*, vol. 31, no. 4, pp. 1738–1747, Aug. 2016.
[33] J. Lyu, X. Cai, and M. Molinas, "Frequency domain stability analysis of MMC-based HVdc for wind farm integration," *IEEE J. Emerg. Sel. Topics Power Electron.*, vol. 4, no. 1, pp. 141–151, Mar. 2016.
[34] N. R. Chaudhuri, R. Oliveira, and A. Yazdani, "Stability analysis of vector-controlled modular multilevel converters in linear time-periodic framework," *IEEE Trans. Power Electron.*, vol. 31, no. 7, pp. 5255–5269, Jul. 2016.
[35] R. Marquardt, "Modular multilevel converter: An universal concept for HVdc-networks and extended dc-bus-applications," in *Proc. Int. Power Electron. Conf.*, Jun. 2010, pp. 502–507.
[36] A. Lopez, D. E. Quevedo, R. P. Aguilera, T. Geyer, and N. Oikonomou, "Validation of a reduced order model for modular multilevel converters and analysis of circulating current," in *Proc. 7th Eur. Conf. Power Electron. Appl., Energy Convers., Congr. Expo.*, 2015, pp. 1–10.
[37] N. Ahmed, L. Ängquist, S. Norrga, and H.-P. Nee, "Validation of the continuous model of the modular multilevel converter with blocking/deblocking capability," in *Proc. 10th IET Int. Conf. AC DC Power Transmiss.*, 2012, pp. 1–6.
[38] N. Ahmed, L. Ängquist, and H.-P. Nee, "Continuous modeling of open-loop control based negative sequence current control of modular multilevel converters for HVdc transmission," in *Proc. 15th Eur. Conf. Power Electron. Appl.*, 2013, pp. 1–10.
[39] R. Trinchero, I. Stievano, and F. Canavero, "Steady-state analysis of switching power converters via augmented time-invariant equivalents," *IEEE Trans. Power Electron.*, vol. 29, no. 11, pp. 5657–5661, Nov. 2014.
[40] S. Norrga, L. Angquist, K. Ilves, L. Harnefors, and H. Nee, "Frequency-domain modeling of modular multilevel converters," in *Proc. 38th Annu. Conf. IEEE Ind. Electron. Soc.*, Oct. 2012, pp. 4967–4972.
[41] D. Jovcic and A. A. Jamshidifar, "Phasor model of modular multilevel converter with circulating current suppression control," *IEEE Trans. Power Del.*, vol. 30, no. 4, pp. 1889–1897, Aug. 2015.
[42] S. Rajesvaran and S. Filizadeh, "Modeling modular multilevel converters using extended-frequency dynamic phasors," in *Proc. IEEE Power Energy Soc. Gen. Meeting*, 2016, pp. 1–5.
[43] J. Peralta, H. Saad, S. Dennetière, J. Mahseredjian, and S. Nguefeu, "Detailed and averaged models for a 401-level MMC–HVdc system," *IEEE Trans. Power Del.*, vol. 27, no. 3, pp. 1501–1508, Jul. 2012.
[44] T. Geyer and D. E. Quevedo, "Multistep finite control set model predictive control for power electronics," *IEEE Trans. Power Electron.*, vol. 29, no. 12, pp. 6836–6846, Dec. 2014.

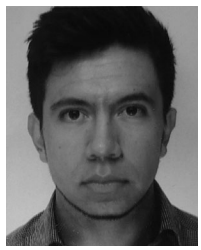

Andres M. Lopez (S'11) was born in Bogota, Colombia. He received the B.Sc. and M.Sc. degrees in electrical engineering from Pontificia Universidad Javeriana, Bogota, Colombia, in 2010 and 2013, respectively, and is currently working toward the Ph.D. degree in model predictive control for modular multilevel converters from Paderborn University, Paderborn, Germany.

He has participated in several research projects including a project supported by the Departamento Administrativo de Ciencia, Tecnología e Innovación (Colciencias), Bogota, Colombia, on power converters for excimer lamps. His research interests include modeling and control of power converters.

Daniel E. Quevedo (S'97–M'05–SM'14) received Ingeniero Civil Electrónico and M.Sc. degrees in electronics engineering from the Universidad Técnica Federico Santa María, Valparaíso, Chile, in 2000, and the Ph.D. degree from the University of Newcastle, Newcastle, NSW, Australia, in 2005.

He is the Head of the Chair of Automatic Control (Regelungs- und Automatisierungstechnik) at Paderborn University, Paderborn, Germany. He was supported by a full scholarship from the alumni association during his time at the Universidad Técnica Federico Santa María. His research interests include control of networked systems and of power converters.

Prof. Quevedo is an Associate Editor of the IEEE CONTROL SYSTEMS MAGAZINE, an Editor of the *International Journal of Robust and Nonlinear Control*, and the Chair of the IEEE Control Systems Society Technical Committee on Networks and Communication Systems. He received several university-wide prizes upon graduating. He received the IEEE Conference on Decision and Control Best Student Paper Award in 2003 and was also a finalist in 2002. In 2009 he was awarded a five year Research Fellowship from the Australian Research Council.

Ricardo P. Aguilera (S'01–M'12) received the B.Sc. degree in electrical engineering from the Universidad de Antofagasta, Antofagasta, Chile, the M.Sc. degree in electronics engineering from the Universidad Tecnica Federico Santa Maria, Valparaíso, Chile, and the Ph.D. degree in electrical engineering from the University of Newcastle (UoN), Newcastle, NSW, Australia, in 2003, 2007, and 2012, respectively.

From 2012 to 2013, he was a Research Academic at UoN, where he was part of the Centre for Complex Dynamic Systems and Control. From 2014 to 2016, he was a Senior Research Associate in the University of New South Wales, Sydney, NSW, Australia, where he was part of the Australian Energy Research Institute. Since September 2016, he has been in the School of Electrical and Data Engineering, University of Technology Sydney, Sydney, NSW, Australia, where he currently holds a Lecturer position. His main research interests include power electronics, renewable energy integration, and theoretical and practical aspects on model predictive control.

Tobias Geyer (M'08–SM'10) received the Dipl.Ing. and Ph.D. degrees in electrical engineering from ETH Zurich, Zurich, Switzerland, in 2000 and 2005, respectively.

From 2006 to 2008, he was with GE's Global Research Centre, Munich, Germany. Subsequently, he spent three years in the University of Auckland, Auckland, New Zealand. In 2012, he joined ABB's Corporate Research Center, Baden, Switzerland, where he is currently a Senior Principal Scientist for power conversion control. In 2017, his habilitation in power electronics was granted by ETH Zurich, and he was appointed as an extraordinary Professor in Stellenbosch University, Stellenbosch, South Africa. He is the author of more than 100 peer-reviewed publications, 30 patent applications, and the book *Model Predictive Control of High Power Converters and Industrial Drives* (Wiley, 2016). He teaches a regular course on model predictive control at ETH Zurich. His research interests include model predictive control, medium-voltage drives and utility-scale power converters.

Dr. Geyer is an Associate Editor of the IEEE TRANSACTIONS ON POWER ELECTRONICS. He received the 2014 Third Best Paper Award of the Transactions on Industry Applications. He also received two Prize Paper Awards at conferences.

Nikolaos Oikonomou (S'00) was born in Thessaloniki, Greece, in 1977. He received the Dipl.Ing. degree in electrical engineering from Aristotle University of Thessaloniki, Thessaloniki, Greece, in 2000, and the Ph.D. degree in electrical engineering from Wuppertal University, Wuppertal, Germany, in 2008.

In 2009, he joined the Corporate Research Center of ABB, Baden, Switzerland. In 2017, he switched to the R&D Department of ABBs Medium Voltage Drives in Turgi, Switzerland. His research interests include control methods for high-power converters and optimized pulse width modulation techniques.